Impact of high and low vorticity turbulence on cloud-environment mixing and cloud microphysics processes

Bipin Kumar[1], Rahul Ranjan[1,2], Man-Kong Yau[3], Sudarsan Bera[1], and Suryachandra A. Rao[1]

[1]Indian Institute of Tropical Meteorology, Ministry of Earth Scinces, Dr. Homi Bhabha Road, Pashan, 411008, India
[2]Department of Atmospheric and Space Science, Savitribai Phule Pune University, Pune, India 411007, India
[3]Department of Atmospheric and Ocean Science, McGill University, Burnside 805 Sherbrooke Street Montreal, Quebec, Canada H3A 0B9

Correspondence: Bipin Kumar (bipink@tropmet.res.in)

Abstract. Turbulent mixing of dry air affects evolution of cloud droplet size spectrum through various mechanisms. In a turbulent cloud, high and low vorticity regions coexist and inertial clustering of cloud droplets can occur in a low vorticity region. The non-uniformity in spatial distribution of size and number of droplets, variable vertical velocity in vortical turbulent structures, and dilution by entrainment/mixing may result in spatial supersaturation variability, which affects the evolution of the cloud droplet size spectrum by condensation and evaporation processes. To untangle the processes involved in mixing phenomena, a three-dimensional direct numerical simulation of turbulent-mixing followed by droplet evaporation/condensation in a submeter-cubed-sized domain consisting of a large number of droplets is performed in this study. Analysis focused on the thermodynamic and microphysical characteristics of the droplets and the flow in high and low vorticity regions. The impact of vorticity generation in turbulent flows on mixing and cloud microphysics is illustrated.

Keywords: Droplet characteristics, High and low vorticity regions, Cloud turbulence, k-means clustering, Degree of mixing.

Highlights:

- Regions of high vorticity are prone towards homogeneous mixing due to faster mixing by air circulation.
- Microphysical droplet size distribution is wider (narrower) in high (low) vorticity volumes.
- Drier environmental air mixing leads initially to higher spectral width.
- k-means clustering algorithm (an unsupervised machine learning technique) is used to identify regions of high vorticity in the computational domain.

1 Introduction

Clouds are a visible manifestation of tiny water droplets or ice crystals in the Earth's atmosphere. They play multiple roles in atmospheric processes, ranging from the radiation budget to the hydrological cycle (Bengtsson, 2010; Grabowski and Petch, 2009; Harrison et al., 1990; Randall and Tjemkes, 1991). The size of clouds may extend from a few meters to several kilometers. However, the suspended droplets that constitute a cloud are much smaller and typically of size 1-20 μm in radius. The journey from a cloud droplet to a raindrop ($\sim 10^3 \mu m$) is a complicated process. Condensation and collision-coalescence, thetwo key

processes involved in the growth of a droplet, are prominent at different stages of a cloud (Rogers and Yau, 1996). For example, up to a size of 15 μm, diffusional-condensation growth dominates, while collision-coalescence is effective when the droplet radius reaches approximately 40 μm (Pruppacher and Klett, 1997). The rapid growth of droplets in the size range 15-40 μm for which neither condensational growth nor collision-coalescence is effective, is poorly understood. This size range has been termed as the condensation-coalescence bottleneck or the size gap (Grabowski and Wang, 2013). The rapid growth of droplets in the 'size gap' is regarded as one of the important unresolved problems in cloud physics. To explain the rapid growth, several mechanisms like entrainment, turbulent supersaturation fluctuations, enhanced collision rates due to turbulence and the role of giant aerosols have been proposed. This study focuses on the interaction between droplets and turbulence to explore how this interaction modifies the droplet characteristics.

1.1 Role of Turbulence in Cloud Microphysics

Understanding the impact of turbulence on the dynamics and microphysics of clouds is a long-standing problem (Devenish et al., 2012; Grabowski and Wang, 2013; Khain et al., 2007; Shaw, 2003; Vaillancourt and Yau, 2000), has been an active area of research using in-situ observations and numerical models. The position and movement of droplets are controlled by turbulent eddies of varying sizes. Simultaneously, evaporation or condensation of droplets incurs changes in the local environment ($\sim$ scale of droplet itself) through latent heat exchange. Additionally, buoyancy generated by phase change (when a bunch of droplets evaporate or condense instead of a few) may impact cloud-scale motions. The inertial response time 'τ_p' is a quantity that determines how quickly droplets respond to the changes in the surrounding fluid motion (Clift et al., 2013). Some droplets are tiny and precisely follow the flow trajectory, while larger ones can modify the flow. Thus, droplet-turbulence interaction is a multi-scale process and is non-local in nature.

There are several macrophysical and microphysical implications of droplet-turbulence interactions. Droplets in the decaying part of a cloud may be transported by turbulence to the more active regions to undergo further growth (Baker and Latham, 1979; Jonas, 1991). The inhomogeneous mixing model used by Cooper et al. (1986) and Cooper (1989) shows that when a parcel of air undergoes successive entrainment events, each of which reduces the droplet concentration, can lead to enhanced droplet growth. However, Jonas (1996) argues that ascent leading to droplet growth may activate some entrained nuclei to limit the maximum supersaturation achieved which in turn limits the droplet growth rate. Vaillancourt et al. (1997) gives further insight into the nature of turbulent-entrainment at the cloud edges. They argue that the interaction between the ambient and the cloudy air is not the same everywhere. There are some prominent regions of entrainment with vortex circulations.

The study of microphysical droplet-turbulence interaction has gained momentum in recent years due to advances in computational capabilities. Several possibilities like turbulence induced supersaturation fluctuation and enhanced collision rates have been investigated. Some studies (Chen et al., 2016; Franklin et al., 2005; Pinsky et al., 2000; Riemer and Wexler, 2005; Shaw, 2003; Vaillancourt and Yau, 2000) indicate an enhanced collision rate in a turbulent environment. Shaw et al. (1998) performed model simulation with a Rankine vortex and found that the preferential clustering of droplets in the low vorticity regions increases the spatially varying supersaturation. On the other hand, droplets in the high vorticity regions experience enhanced supersaturation and grow faster. This work laid the foundation for droplet clustering in clouds and its effect on affecting the

droplet size distribution. However, Grabowski and Vaillancourt (1999) commented on the limitations of applying Shaw et al. (1998) results to atmospheric clouds, because of the absence of droplet sedimentation, the assumption of high volume fraction of vortex tubes (50%) and the strong dependence on the vortex lifetime.

There is no clear theory regarding vorticity characteristics in three-dimensional homogeneous turbulent flows, despite increasing research on turbulence. Vorticity has a profound impact on the spatial distribution of droplets. Due to preferential clustering, relatively fewer droplets are left in high vorticity regions (Karpińska et al., 2019). The difference in the spatial distribution of droplets induces supersaturation fluctuations. The low number of droplets competing for the available vapour field in high vorticity regions should experience enhanced growth. However, for this to happen, droplets should stay in these regions for duration long enough for the supersaturation field to act. In general, little is known about the length and lifetime that the high vorticity regions occupy (Grabowski and Wang, 2013). Due to these limitations, the effect of preferential clustering on the diffusional growth of droplets is poorly understood.

In this study, we examine the diffusional growth and evaporation of cloud droplets in an entrainment and mixing scenario using Direct Numerical Simulation (DNS). We compare the droplet characteristics such as spectral width, volume mean radius, number concentration, probability density function of droplet radii and supersaturation in high and low vorticity regions. As reported by Vaillancourt et al. (1997), the main entrainment sites and mixing zones were located in the vortex circulation areas. Accordingly, we aim to look for, using DNS, locations with vortex circulations in the main entrainment sites and mixing zones. In summary, the main purpose of this study is to seek answers to the questions regarding the amount of high intensity vortices in a turbulent domain and the dominant locations of mixing in the high and low vorticity regions. Specific scientific questions targeted in this work are; (i) variations of droplet spectral properties in high and low vorticity regions, (ii) quantification of the degree of mixing in these regions and (iii) the impact of relative humidity in the evolution of the droplet size spectra.

The organisation of the paper is as follows. The next section provides details of the methods and data used. Results and discussions are provided in section 3 with further four subsections containing the discussion of the flow and the droplet characteristics in low and high vorticity regions. In the last part, we concluded our findings.

2 Data and Methods

We carried out a DNS following the setup of Kumar et al. (2014, 2018) to simulate the entrainment and mixing mechanisms at cloud edges. This DNS code uses the Euler-Lagrangian frame, solves the flow equations at each grid point, and tracks each droplet inside a grid by integrating the equations for its position, velocities, and growth rate. The simulation produces the output in two formats, one is from the Eulerian frame in NetCDF format developed by UCAR/Unidata and the other is the droplet dynamics output saved in SION format (SIONLib, 2020). The simulation domain was chosen $(51.2cm)^3$ with $1mm$ grid resolution, thus containing a total $(512)^3$ grid points in the domain. An initial setup of the computational domain is detailed in section 3.

Two simulation setups were considered in this study. In particular, there are two relative humidity (RH) cases (85% and 22%) initialized with a poly-dispersed droplet size distribution. We have also attempted two simulations (two RH cases) initialized

by a mono-dispersed droplet size (20 μm). However, our discussion is focused only on the results from the poly-dispersed case as the mono-dispersed case does not provide any additional results. The poly-dispersed set up contains droplet size distribution (size range 2-18 μm) from cloud observation (CAIPEEX experiment: https://www.tropmet.res.in/ caipeex/) used in Kumar et al. (2017) with a mean radius of $9.3\,\mu m$. The two humidity corresponding to dry (RH=22%) and moist air (RH=85%) were taken from observations of the monsoon environment (Bera et al., 2016). A supersaturated cloudy slab in the DNS domain is specified to simulate the mixing processes.

This study aims to investigate droplet characteristics in high and low vorticity regions in cloud turbulence. Therefore, the vorticity magnitudes were first calculated using the Eulerian data at each grid point containing the velocity components in the X, Y and Z directions. The next step is to find the high and low vorticity regions in the DNS computational domain. It requires calculating and visualizing the actual vortices generated by the turbulent flow. Since the grid size is $1\,mm$, it is not feasible to obtain a vortex inside a single grid box; instead, a volume containing the vortex must be sought, encompassing multiple grid boxes. It is a challenging task to locate a small box to cover a minimal portion of the low vorticity region. We used an unsupervised machine learning (ML) algorithm mentioned in the next subsection to address this problem.

2.1 Locating High Vorticity Regions

To locate high vorticity regions in the domain, we used the k-means clustering algorithm from Scikit-Learn python package (Pedregosa, 2011). The k-means clustering (Bock, 2007) is one of the most popular and the simplest unsupervised machine learning algorithm. It makes 'k' groups or clusters from a dataset based on the Euclidean distance between individual data points. However, k-means clustering cannot guess the optimum number of clusters for a particular dataset; instead, the user has to assign it. Therefore, selecting the number of groups or clusters in which a dataset has to be grouped or clustered is crucial. This algorithm was used to locate high vorticity regions from the vorticity data.

The absolute vorticity ω related to the velocity components is calculated as (see Chapter 4.2 in Holton and Hakim (2013))

$$\omega = (\omega_i^2 + \omega_j^2 + \omega_k^2)^{\frac{1}{2}} \tag{1}$$

where

$$\omega_i = \frac{\delta w}{\delta y} - \frac{\delta v}{\delta z}; \qquad \omega_j = \frac{\delta u}{\delta z} - \frac{\delta w}{\delta x}; \qquad \omega_j = \frac{\delta v}{\delta x} - \frac{\delta u}{\delta y} \tag{2}$$

The values of ω, in our DNS data, range from $0 - 200\,s^{-1}$ as seen in panel (a) of Figure 1. Vaillancourt and Yau (2000) mentioned that only a small fraction of the cloud core is occupied by high vorticity regions and no preferential concentration of cloud droplet was observed there. We also found that less than 2% of the grids (by volume) have vorticity with magnitude greater than $60s^{-1}$. For larger vorticity magnitudes even fewer numbers (almost negligible) of grids were located. Based on these findings, in this work, a threshold value of vorticity magnitude, $60s^{-1}$ was chosen as high vorticity criterion. We also investigated the droplets characteristics with a threshold of $50s^{-1}$ either difference in the trends. We also mention that using

$30s^{-1}$ as a threshold for high vorticity, which is less than $1/5^{th}$ of the maximum vorticity magnitude ($200s^{-1}$), does not seem to be justified. Figure 1(b) depicts the fraction of grid points for different threshold values of vorticity magnitude.

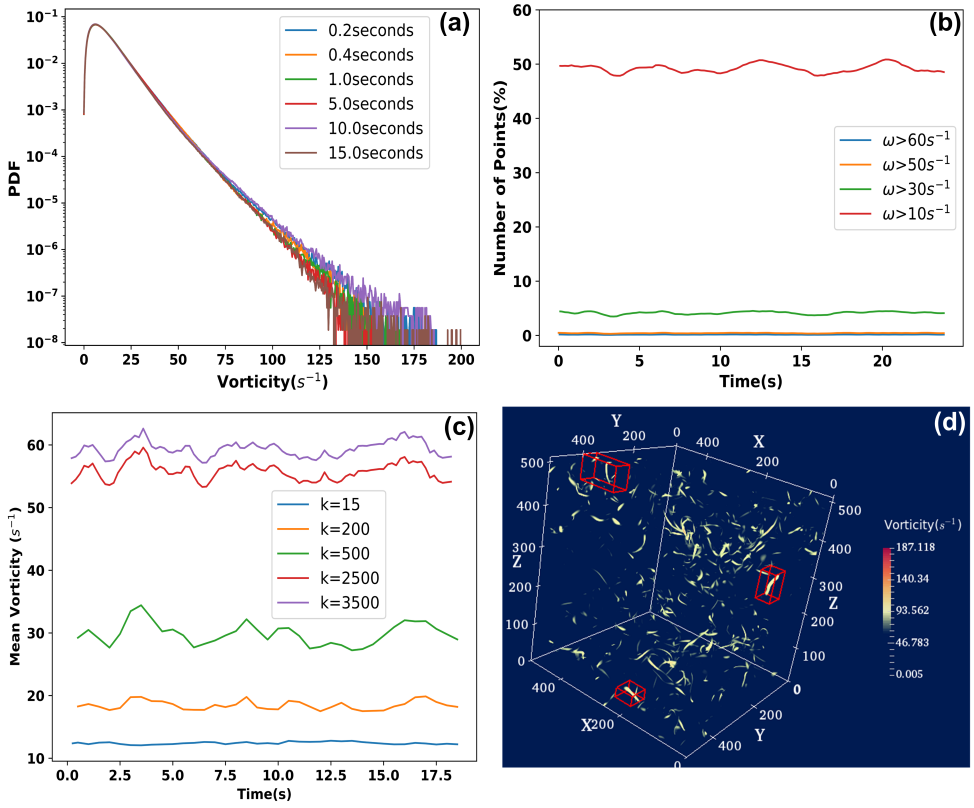

Figure 1. The panel (a) displays the PDF of vorticity at different times. The fraction of high vorticity points (based on threshold values) are depicted in panel (b). Panel (c) represents vorticity values for different values of 'k'. Panel (d) shows high vorticity regions (enclosed by rectangular cuboid) obtained for k=500.

Once the threshold value for vorticity magnitude is decided, the next step is to locate 3D boxes enclosing the high vorticity regions. We look for these regions at every time step. To locate the boxes having high vorticity, we applied a machine learning algorithm, namely, k-means clustering. Wherein, two input variables have to be assigned a value; (i) the number of clusters ('k') and (ii) the maximum number of iterations. Since vortexes have tubular or sheet type structures, it is possible that a 3D box may contain many low vorticity points for a typical value of 'k'. Hence, an optimal value of 'k' is required to select small enough 3D boxes to avoid the low magnitude vorticity points.

We identified the value of 'k' to be used in the algorithm by conducting several experiments and selected the optimal value k=3500 based on the chosen threshold value for high vorticity. At k=3500, the average vorticity in the boxes reach is close to the selected threshold ($60s^{-1}$), as shown in Figure 1(c). This figure provides the vorticity values for different values of 'k' and confirms the appropriate choice of k=3500. The value of 'k' also affects the size of the cluster. With increasing value of 'k', the

size of the clusters decreases. Consequently, some clusters may become so small that they may include as many as two or three (say) high vorticity points only, all in the same plane. These points in the same plane will not be useful as they cannot form a cuboid. Therefore, the 'k=3500' value was found to be optimal. For a higher value of 'k', we may get many zero volume boxes. That is the reason why increasing the value of 'k' indefinitely is not advisable. Similarly, the optimal numbers of iterations were chosen as 200 to keep the computational cost moderate. A typical visualization of finding a volume enclosing a high vorticity region is shown in Figure 1(d), where a cuboid is shown to surround the high vorticity region. It was noted that high vorticity regions occupy only a tiny fraction (0.1- 0.2 %) of the total domain.

Set up	**Shaw et al. (1998)**	**This study**
Entrainment-Mixing	No	Yes
Vortex Lifetime	2-3 orders of magnitude > Kolmogorov timescale (≈10 sec)	Less than 1 sec
Volume fraction of high vorticity	$\approx 50\%$	less than 2%

Table 1. A comparison of this study with the previous study of Shaw et al. (1998) which laid the foundation for droplet clustering and their effects on the droplet size distribution. Kolmogorov time scales in natural clouds are in the range of $0.01 \rightarrow 0.1$ seconds. Kolmogorov time scale for DNS is 0.0674 seconds, which lies in the said range.

This finding of a tiny fraction for high vorticity regions in a cloud core is in agreement with the DNS study of Jimenez et al. (1993) and Vaillancourt and Yau (2000) but disagrees with the assumed high volume fraction ($\approx$ 50%) by Squires and Eaton (1991) and later by Shaw et al. (1998). There are important differences between this study and the study of Shaw et al. (1998), who laid the foundation of inertial clustering of cloud droplets and motivated us to conduct the present study. Shaw et al. (1998) hypothesized that the preferential concentration (inertial clustering) occurs at small spatial scales and low (high) particle concentration corresponds to high (low) vorticity regions using a Rankine vortex in their model. They assumed a high fraction (50%) of vortex structure and the preferential concentration of droplets was several folds higher than the mean droplet concentration. In contrast, the high vorticity region in the present simulation is very small (≈0.2% volume fraction) with about 1.5 fold higher droplet concentration than in the low vorticity region.

A comparison of the methods in this work and the study of Shaw et al. (1998) is provided in table 1. For calculating the volume fraction of high vorticity region, Shaw et al. (1998) considered two zones of vortices (high and low vorticity) in their parcel model with a Rankine vortex and considered the same volume fraction (i.e., 50%) for the two vorticity zones.

3 Results and discussion

In this section, we discuss the various analyses from the two humidity simulations initialized with a poly-dispersed droplet size spectrum.

3.1 Initial simulation setup

The interface between cloud volume and the sub-saturated air is distinguishable during the early evolution of the flow. To see if any features of the flow exhibit distinct properties at the edges, three separate volumes from the entire domain have been selected. The cloudy slab area lies between 142mm to 372mm along the x-axis, with the rest of the domain occupied by the

sub-saturated air. Of the two interface volumes, one is on the left side (between $x = 70\,mm$ to $140\,mm$), and the other is on the right side ($x = 364\,mm$ to $434\,mm$). The volume lying between $x = 182\,mm$ and $322\,mm$ is in the core region, as depicted in Figure 2.

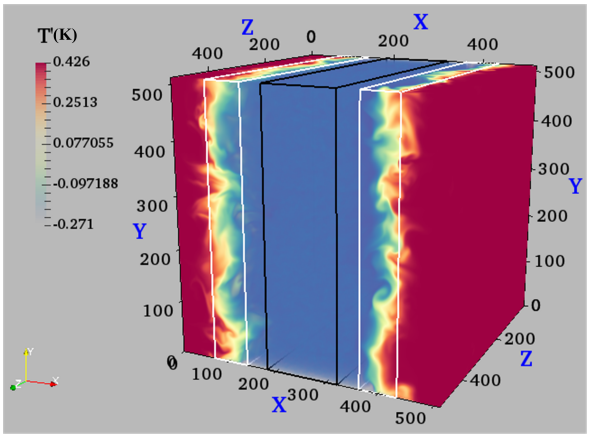

Figure 2. The snapshot of DNS domain at 0.2 seconds time which can be considered as the initial state of the simulation. It also shows two boxes, particularly at the edges (left and right white boxes) and the initial cloud slab (central black box). The legends represent fluctuations from mean temperature.

3.2 Turbulence characteristics at the edges and core of cloud

The cloudy volume properties initially see sharp changes, which was confirmed by analysing the variations in kinetic energy (KE), vorticity, and mixing ratio. The edges are the most turbulent part of the clouds during the early evolution time; and considerable robust fluctuations in KE are experienced there, as depicted in the upper panel of Figure 3. The availability of more kinetic energy at the cloud edges makes them the hotspots for vorticity generation. Initially, a higher value of mean vorticity is observed at the edges in both humidity cases, evident in the lower panel of Figure 3. Near the edges, strong gradients of mixing ratio and temperature exist, leading to the generation of instabilities and consequently, turbulent mixing. TKE is initially associated with the vortical motions at the interface, however, additional TKE is also generated due to negative buoyancy production by droplet evaporation. This energy is transported to the cloud slab as time progresses by the vortices ('eddies') that propagate inward. However, there are periodic changes in the TKE variations between the interface and the cloud slab possibly due to the periodic boundary condition of the DNS setup. A notable feature between the two RH simulations (22% and 85%) is the larger difference in vorticity between the interface and the cloud slab in the drier case (RH=22%) due to strongest evaporation.

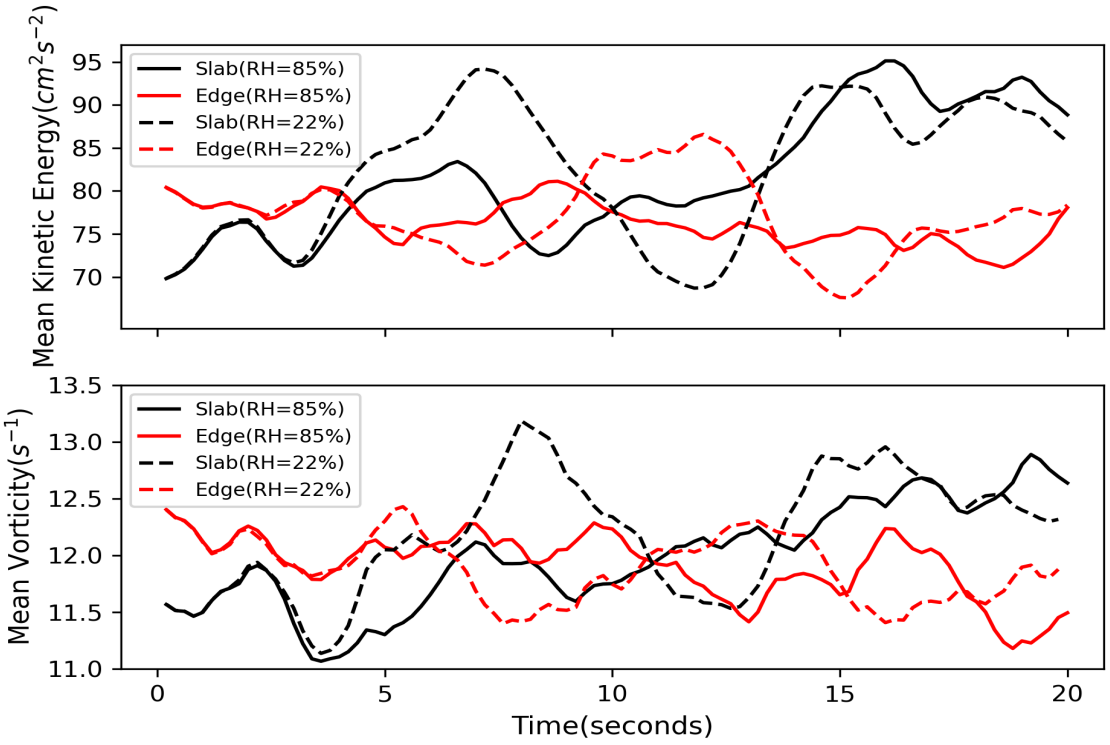

Figure 3. Upper panel is for the variation in kinetic energy (KE) for both drier and humid cases in the cloudy slab and edges. Mean vorticity variations at the edges and within the cloudy slab, in both cases, is shown in the lower panel. The KE was averaged over cloudy slab and both drier edges. The vorticity averaged was taken in each box enclosing them.

3.3 Flow characteristics in high and low vorticity regions

The previous subsection presented the variation in flow characteristics at the cloud core and the edges. Another part of this study is to investigate these characteristics in the high vortex (HV) regions of the turbulent flow, with a vorticity magnitude greater than $60\,s^{-1}$. Similarly, points with vorticity less than $30\,s^{-1}$ were classified as regions of low vorticity (LV).

We also investigated the evolution of the vapor mixing ratio (q_v) in both the drier (RH=22%) and the more humid cases (RH=85%). The incursion of drier air results in a lower mixing ratio at the edges as evident from the left panel of Figure 4. In both HV and LV regions, we further determined the root mean square velocity U_{rms}. For the dry and humid cases, U_{rms} is found to be higher in HV regions as depicted in the left panel of Figure 4.

3.4 Droplet Characteristics

One of the main aims of this study is to examine various droplet characteristics such as number concentration, volume mean radius, spectral width, and the mixing process in HV and LV regions. This subsection focuses on all these characteristics.

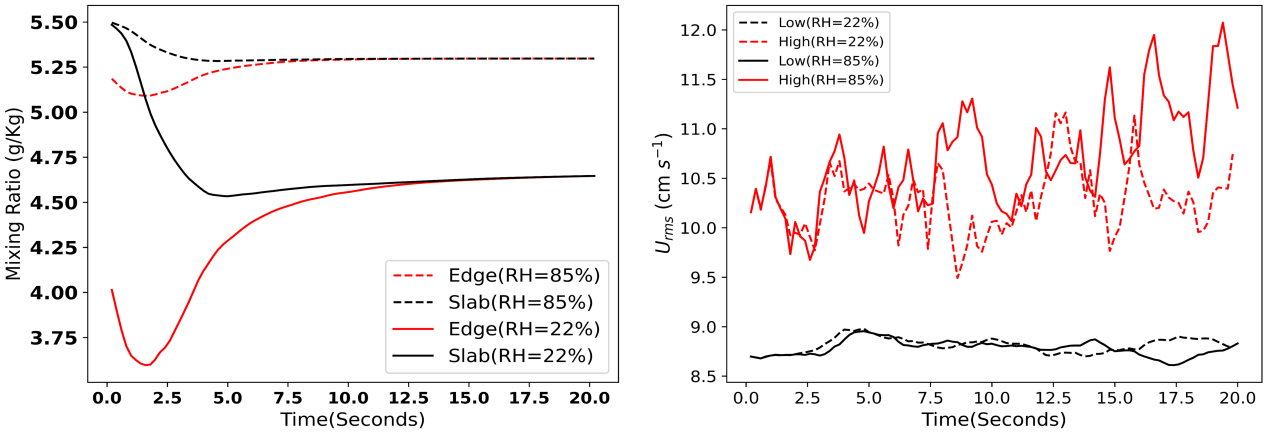

Figure 4. Evolution of vapor mixing ratio is depicted in the left panel. Right panel represents the variation in U_{rms}.

3.4.1 Number concentration and mean volume radius

There have been many kinds of research on the distribution of droplets in a turbulent flow field. Several laboratory studies (Lian et al., 2013) and model simulations (Shaw et al., 1998; Ayala et al., 2008) reported on the process of preferential clustering of cloud droplets in low vorticity regions. The preferential clustering means that droplets prefer to cluster in some specific flow regions rather than randomly distributed everywhere. A high amount of rotation characterizes the highly vortical part of a fluid. When a droplet enters this region, it is flung out due to its inertia and accumulates in a low vorticity region. This process leads to a heterogeneous droplet concentration in space, an important aspect that affects the droplet growth rate and the size distribution. In a poly-dispersed size distribution, the larger droplets are more prone to be affected by the vorticity compared to smaller droplets that may follow the flow streamline due to their low inertia. For this reason larger droplets accumulate in low vorticity regions and result in larger mean volume radius.

In the upper panel of Figure 5, both humidity cases show almost the same trend, i.e., a higher number concentration in the low vorticity region due to inertial clustering. The lower panel of Figure 5 shows variation of mean volume radius in high and low vorticity regions. Arid like condition in the case with RH=22% leads to fast evaporation of droplets as indicated by the rapid decay in the droplet number concentration and the mean volume radius. Consequently, the number concentration curves almost merge after 7.5 seconds. Due to preferential clustering, the high vorticity regions have a relatively small number of droplets. It is to be noted that the low vorticity region always has larger mean volume radius during the simulations as shown in the lower panel of Figure 5.

There may be two possible reasons for the smaller value of the mean radius in high vorticity regions: (i) droplets experience a drier environment and evaporate faster during the early stage of mixing when high vorticity forms at the cloud edge, and (ii) larger droplets are favored to be flung out of the high vorticity region as a consequence of greater inertia effect, leaving behind only the smaller ones, i.e., preferential clustering is more prominent for larger droplets. The second possibility is more valid

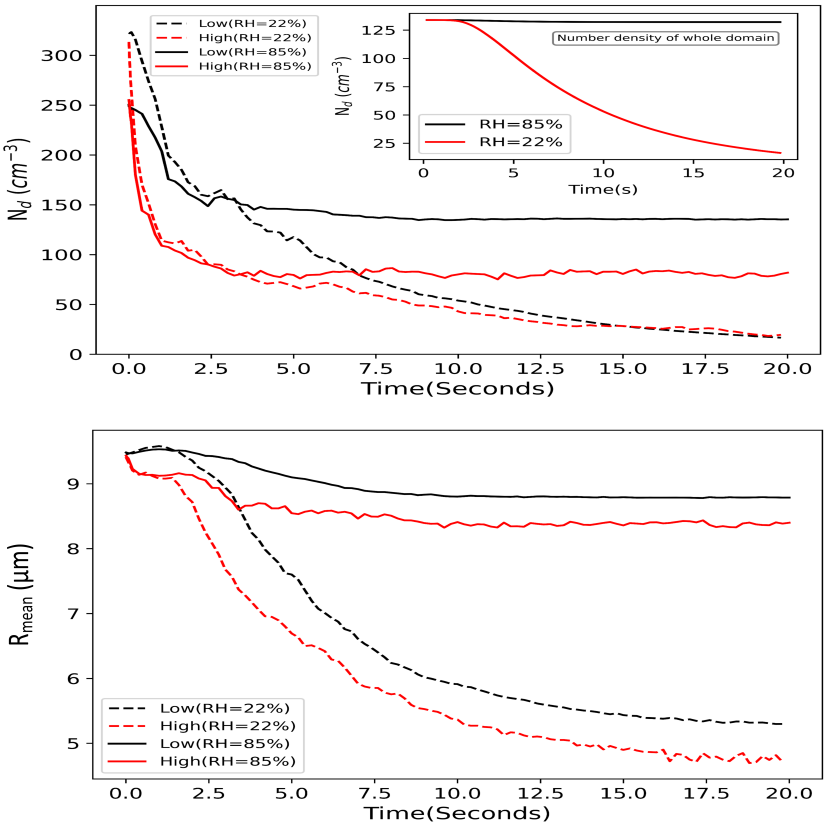

Figure 5. Evolution of number concentration (N_d) in the whole domain (the inner panel) is shown in the upper panel. In both RH cases, initial number densities (in the entire domain) were close to $130\,cm^{-3}$. However, the evolution of N_d in high and low vorticity regions have different magnitudes. It is always greater in the low vorticity regions. The lower panel shows the volume mean radius which is always smaller in the high vorticity regions.

during the later part of the simulation (approx. after 5 sec) when high vorticity forms inside the cloud slab. To clarify whether preferential clustering alone determine the volume mean radius distribution or whether the other mechanisms are responsible, we investigated the droplet spectra, the trends of the mean supersaturations, and the evolution of the droplet size distribution.

3.4.2 Evolution of Droplet Size Spectra

The variation of the spectral width is presented in the left panel of Figure 6, showing an entirely different picture of the evolution of droplet spectra in the two cases. The right panel of this figure illustrates the dispersion of the droplet size distribution.

During the initial mixing of the cloud slab with the environmental dry air in the RH22% case, the spectral width of DSD increases rapidly up to the 5-7 seconds and then decreases thereafter. Whereas in the RH85% case, a gradual increase can be seen for the initial 10 seconds and remains almost constant after that. One of the most important results of this study is that the spectral width of DSD is different in high and low vorticity regions as depicted in figure 6. The droplet size dispersion also

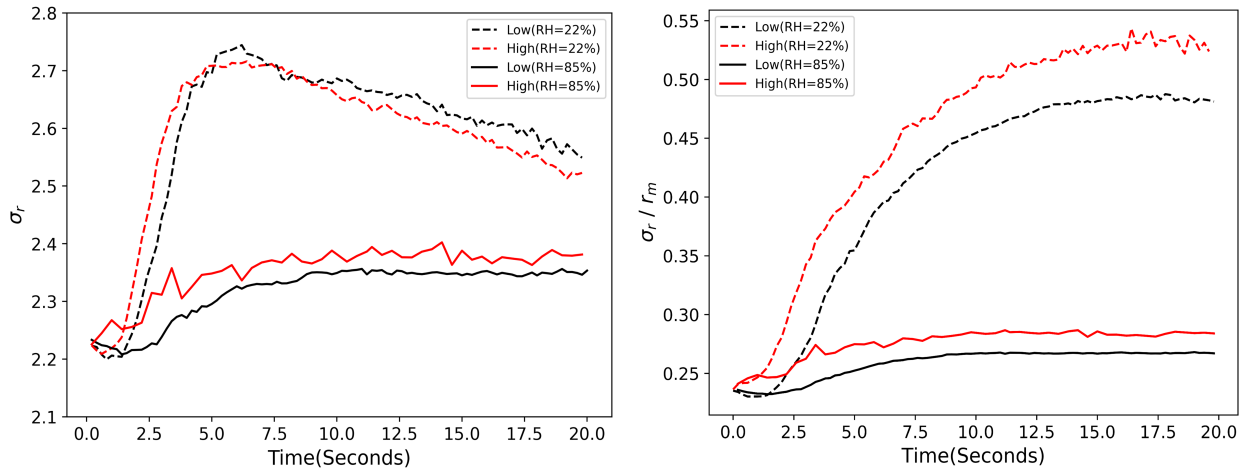

Figure 6. Variation of spectral width in high and low vorticity region is shown in left panel. The spectral width is always greater in the high vorticity region in the RH85% case while it is greater for the initial 5 seconds only in RH22% case. Right panel depicts the variation of dispersion of the droplet size distribution with time.

confirms that the broadening is always stronger in the high vorticity regions. For the RH22% case, spectral width is wider for droplets situated in high vorticity region during the initial 5 seconds of mixing when the spectral width increases rapidly. But the opposite scenario occurs after 7.5 seconds i.e., narrower spectral width in high vorticity regions. Nevertheless, the spectral width is always wider in the high vorticity regions in the RH85% case.

The initial growth and later decay of the spectral width during mixing for the RH22% case is associated with the modification of the spectral shape by droplet evaporation and the number concentration dilution (see Bera (2021)). In this case, evaporation is very significant due to the mixing of the much drier environmental air. When evaporation starts, the smaller droplets of the DSD evaporate faster compared to the larger droplets in accordance with the inverse relation of growth rate with droplet size (Rogers and Yau, 1996). As a result, the spectra shift towards the smaller size tail as shown in the upper panel of Figure 7. This is the reason for the increasing spectral width for the initial 5 seconds in RH22% and during the entire 20 seconds of RH85%. However, when evaporation is such that the smaller size tail of the spectra is evaporated completely and only larger droplets remain, the spectra start to shrink and the spectral width decreases as shown in Figure 7 (c) (see Luo et al. (2020)) . This is the situation for RH22% with mixing after 7.5 seconds but does not occur for RH85% case where the evaporation is much slower due to moist air mixing (as shown in Figure 7 (d)).

The difference of the spectral width in the HV and LV regions can be by higher droplet evaporation in high vorticity regions. Initially, high vorticity forms at the cloud edges where dry air mixing occurs, leading to faster evaporation of droplets. A second possibility is that high vorticity regions are pockets of rotating air motions that can easily transport the vapour mass (produced by droplet evaporation) out of the region to facilitate enhanced evaporation. These two plausible reasons result in higher evaporation rate in regions of high vorticity and consequently impact of the droplet spectral width.

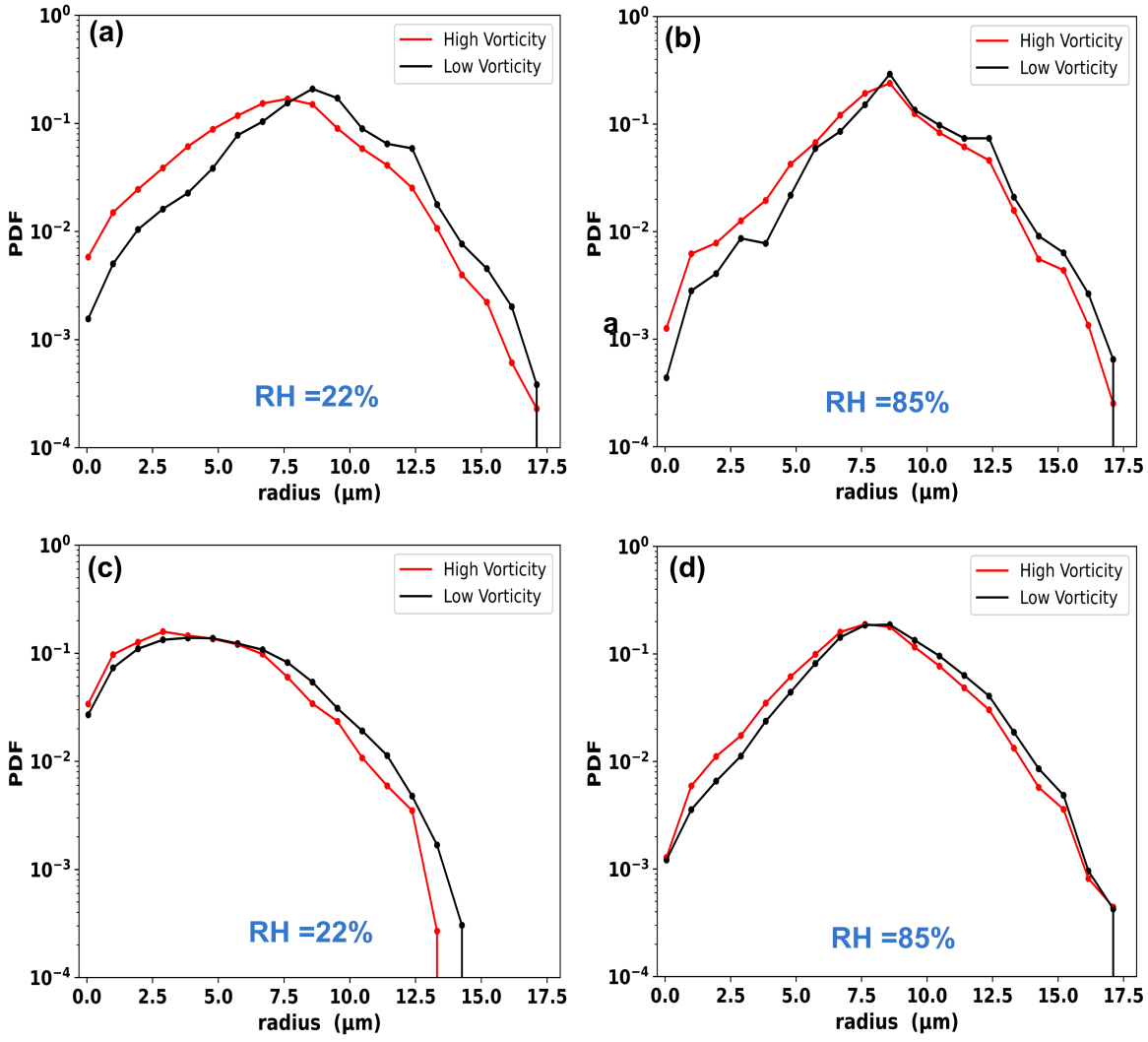

Figure 7. Probability density function of droplet radii for 22% RH (left panel) and 85%RH (right panel). Upper panel depicts the plots for 3 seconds and the bottom one is for 17.8 seconds.

The differences in the PDFs of HV and LV regions can be noticed very well at 3 and 17.8 seconds. During this time, a greater spectral width exists in the high vorticity region (refer to figure 6) for both humidity cases (i.e., RH=22% and RH=85%). The PDFs confirm that high and low vorticity regions contain almost the same maximum and minimum drop sizes, but the difference comes from the distribution. The following possibilities can explain the characteristics of the PDF depicted:

- Saturation ratio is lower in high vorticity regions, which triggers enhanced evaporation.
- Due to enhanced evaporation, there are smaller droplets in the vortices as depicted by the size distribution.
- Bigger droplets are more vulnerable to be thrown out of the vortices, leaving only the smaller ones.

For further understanding, we also analysed the trend of the droplet supersaturation as follows.

3.4.3 Mean saturation ratio

Figure 8 depicts the mean and standard deviation of supersaturation variation in HV and LV vorticity regions for RH=22% and 85% cases. The droplets in high vorticity regions experience comparatively lower saturation ratio until around 6 seconds, after which the difference tends to vanish. Hence, during entrainment of drier air into the cloudy volume, droplets encounter a more sub-saturated environment in the highly vortical regions, and it is the lower saturation ratio values that produce a larger standard deviation. In RH22% case, the saturation ratio drops to -15%, while in RH85% case, although a similar pattern exists, the saturation ratio drops only up to -3%. In summary, the high vorticity regions can be identified as zones of entrainment.

3.4.4 Degree of mixing

One of the best metrics to investigate the entrainment and mixing process is the degree of mixing, which depends on the mixing diagram and has wider application in numerical models (Lehmann et al., 2009; Kumar et al., 2017, 2018). In the mixing diagram, the volume mean radius cube (r^3) is plotted against the number concentration (N_d). Sometimes, a normalized version is plotted, in which the radius and number concentration are normalized by the respective adiabatic values (Gerber et al., 2008; Kumar et al., 2014) . In a similar manner, we performed the mixing diagram calculation and depicted the values in Figure 9 (a & b). Here, we have considered the initial values (t=0s) as adiabatic in the mixing diagram.

An analysis of the mixing diagrams in the high and low vorticity regions for both the moist and dry cases were performed. Variations in mixing diagrams in high and low vorticity regions for the RH22% case are depicted in panels (a) and (b) respectively in Figure 9. The mixing diagrams, for both RH cases, show a clear picture of mixing types. In the low vorticity case, the mixing is inactive up to 1.2 seconds while for HV case it remains inactive up to 1.4 seconds. During this time, entrained air just dilutes the number concentration (n_h) without acting on droplet evaporation (because the cloudy slab expands during this time and droplets scatter into the entire domain). Afterward, physical mixing occurs, the mixing line takes takes a turn toward the homogenous mixing line (vertical line representing constant number concentration) and both the number density and the mean volume radius decrease rapidly, indicating an intermediate or transient type mixing scenario.

One can summarize that in HV regions the mixing remains more homogeneous compared to LV regions as can be seen by the more rapid droplet evaporation (decrease in r) than the decrease in number density.

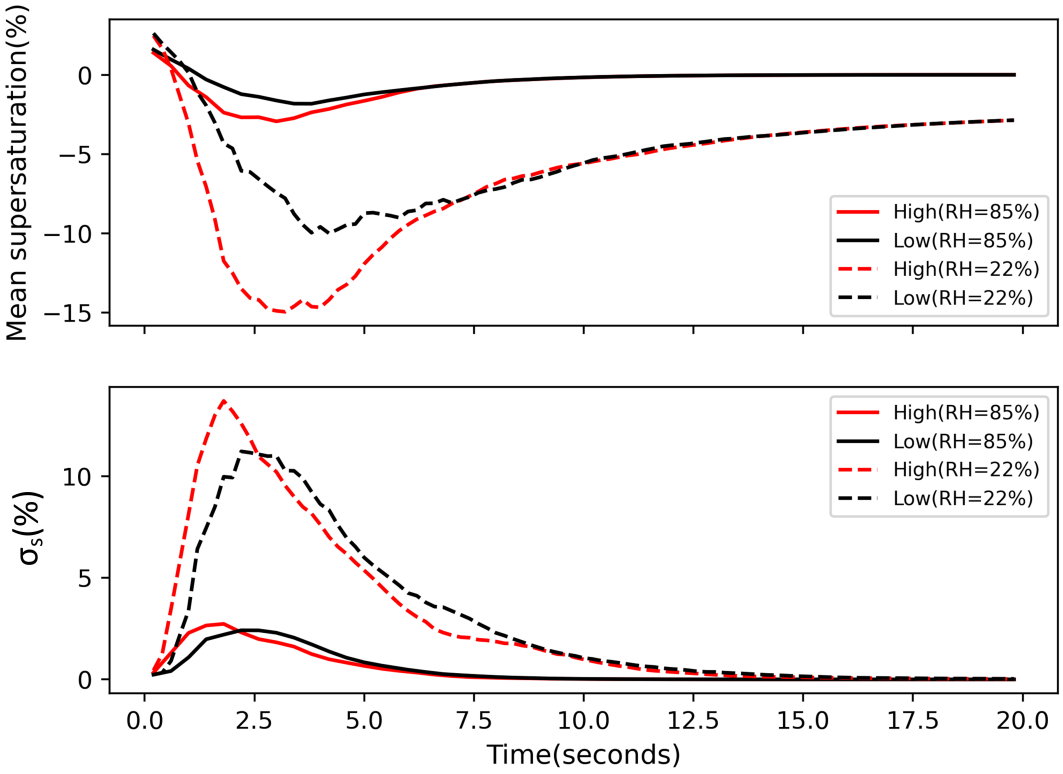

Figure 8. Upper panel is for the evolution of mean saturation ratio in high and low vorticity regions. Saturation ratio is lower in the high vorticity regions during initial 5-7 seconds and its value reaches a minimum of -15% in the RH22% case, while it drops only upto -3% in the RH85% case. Evolution of the standard deviation of saturation ratio in high and low vorticity regions is shown in lower panel. The standard deviation sees a steeper increase and decrease in high vorticity regions, and has a large variation (0-14) in RH22% case, while the variation is small (0-2.8) in the RH85% case.

The degree of mixing was calculated using the following formula from (Lu et al. , 2012), which is based on a 'β' parameter,

$$\beta = tan^{-1}\left\{\frac{\frac{r^3}{r_a^3}-1}{\frac{n}{n_a}-\frac{n_h}{n_a}}\right\} \tag{3}$$

β is normalized by $\pi/2$ to obtain a mixing degree which varies between $[0,1]$. In this equation, r is the mean volume radius, r_a stands for the adiabatic volume mean radius, n, n_h and n_a are the number concentration, homogeneous number concentration, and adiabatic number concentration respectively.

The degree of mixing is presented in Figure 9(c). It is calculated using equation 3 (Lu et al. , 2012). The values of the degree lies in the range $[0,1]$. The value 1 represents homogeneous mixing and extreme inhomogeneous mixing has a zero value. We observed a higher mixing degree in the HV regions in both RH cases. The moist case shows relatively inhomogeneous

mixing initially for both LV and HV regions and gradually shifts towards homogeneous mixing although the HV region always remains at the higher side of homogeneous mixing.

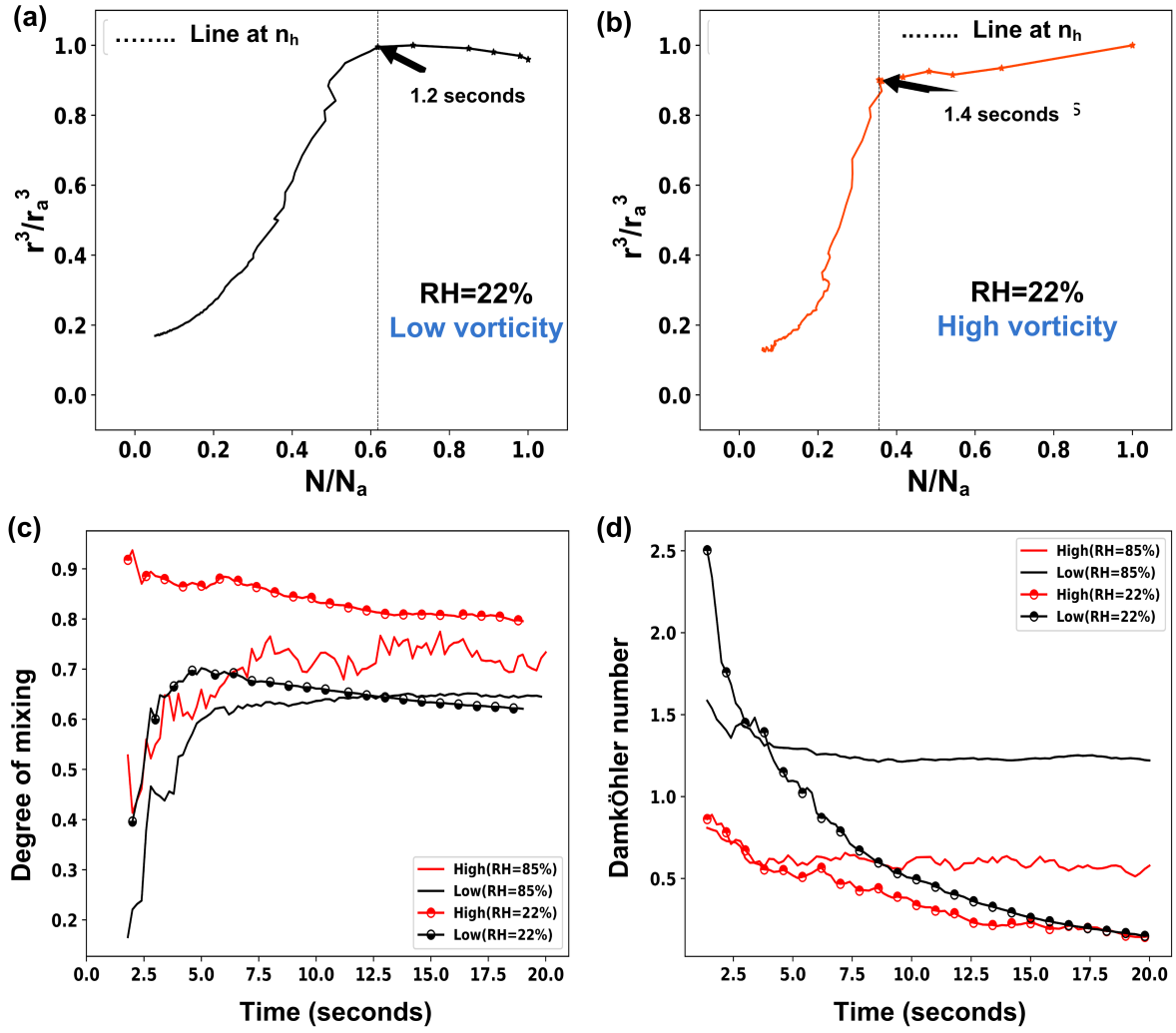

Figure 9. The panel (a) and (b) represent the mixing diagrams for low and high vorticity respectively for RH=22% case. The 'n_h' represents homogeneous number concentration used in equation 3 .Degrees of homogeneous mixing for all four cases are compared in panel (c). A comparison of Damköhler number for all the cases is shown in (d).

280 A comparison of Damköhler numbers for all four cases is presented in panel (d) of Figure 9. The Damköhler number also measures the degree of mixing as a quantity related to two time scales, namely, fluid time scale ($\tau_{fluid} = L/U_{rms}$) and phase relaxation time scale ($\tau_{phase} = \frac{1}{4\pi n_d Dr}$) (Kumar et al., 2012), where U_{rms} is root-mean-square of the turbulent velocity fluctuation, L is a characteristic length (energy injection) scale of the flow, n_d is the droplet number density, 'D' is the modified diffusivity, and 'r' denotes volume mean radius of the droplets.

The Damköhler number, $Da = \tau_{fluid}/\tau_{phase}$, represents an estimation of the mixing scenario. $Da >> 1$ indicates an inhomogeneous process, while $Da << 1$ represents a homogeneous one (Latham and Reed, 1997). In panel (d) of Figure 9, the evolution of the Damköhler number has been shown. Low vorticity regions always have a bigger Da than high vorticity ones. A value closer to 0 indicates a higher degree of homogeneous mixing. Like the mixing diagrams, the Damköhler number also suggests a greater homogeneous mixing in the high vorticity regions. High vorticity (i.e., circulations of fluid) indeed helps to promote faster mixing and produce a well mixed homogeneous cloud volume.

4 Conclusions

Droplet characteristics in high vorticity (HV) and low vorticity (LV) regions in a three dimensional DNS of cloud-environment mixing in cumulus clouds have been studied. We have taken initial (poly-dispersed) drop size distributions, from the CAIPEEX observation (Bera et al., 2016) . Entrainment simulations were performed with two initial relative humidity values viz. 22% and 85% for the ambient air that mixes with a cloud slab.

A DNS model setup similar to Kumar et al. (2014) has been considered. This setup has a cloudy volume and surrounding sub-saturated air, which are allowed to mix as the entrainment simulation kicks in. During the entrainment and mixing process, the flow in the domain develops spatially varying characteristics. The magnitude of turbulence (decaying with time) is not the same everywhere. Some regions are highly turbulent and possess a high value of vorticity. The vortices may influence the distribution and growth of cloud droplets. To study the dependency of droplet characteristics on vorticity, we located HV regions in the computational domain. Finding HV regions is challenging because the shape, size, and position of the vortices change within a fraction of a second. We have applied an unsupervised machine learning algorithm, k-means clustering, to categorize the high and low vorticity clusters. To our knowledge, it is the first time that the machine learning algorithm for investigating cloud turbulence properties has been applied. We answered the following scientific questions in this study

(i) How much volume fraction does intense vorticity occupy in the domain?

(ii) Where is the cloud-clear air interaction most prominent; in highly turbulent regions or weakly turbulent regions?

(iii) Is preferential clustering the same for all droplets sizes? How do the spectral properties of droplets vary in high and low vorticity regions?

(iv) Does the relative humidity of the ambient air have any impact on the evolution of the droplet size spectra?

(v) What is the maximum characteristic, i.e., homogeneity of mixing degree in high vorticity and low vorticity regions?

Entrainment and mixing is a turbulent process, and during the initial few seconds, the cloud edges, where a large gradient of water vapor field exists, are the most turbulent. More robust KE fluctuations were found at cloud edges, making them hotspots for vorticity generation. A distinct difference in the KE fluctuations was noted between two RH simulations (22% and 85%), a bigger difference was observed in the drier (RH=22%) case. Turbulent velocity fluctuations U_{rms} was found higher in HV regions for both simulation cases.

Droplets tend to cluster in the LV region with smaller droplets showing less tendency for the same, which may lead to heterogeneous number concentration in space and time, consequently affecting the droplet size distribution. Clustering of larger droplets in the LV region resulted in a higher mean volume radii over there. The most important result from this study is the different spectral widths (σ_r) in the HV and LV regions. In the drier case, a higher value of σ occurred in HV region during the first 5 seconds, and after that the opposite scenario was observed. This opposite behavior can be connected to droplet evaporation and dilution of the number concentration in the HV region. More air circulation in HV region leads to more incoming drier ambient air as well as more outgoing moist air (as a result of droplet evaporation) from the region to promote much faster droplet evaporation. The spectral width always remains higher in the HV area for the moist case (RH=85%), it may be because of higher droplet evaporation influenced by the presence of rotating air pockets, helping to transport the vapor mass out of the HV region.

The intrusion of subsaturated air is most prominent in the high vorticity regions which reflects in the evolution of the droplet supersaturation. Enhanced evaporation produces a wider droplet and supersaturation spectra. The time series of the droplet number concentration and the volume mean radius can be used to obtain mixing diagrams of high and low vorticity regions. The degree of mixing calculated based on the mixing diagram shows more mixing homogeneity in the HV regions. The Damköhler number which depends upon fluid and phase time scales also indicate a higher degree of homogeneous mixing in HV regions. We emphasize that our findings are strongly affected by entrainment and mixing of drier air at the cloud edges. The results may differ in adiabatic cloud cores where entrainment and mixing are absent.

Data availability. The DNS output data used in this study is archived in HPC Aaditya at IITM pune and can be made available on request.

Author contributions. BK and MKY formulated the concept of this work. BK prepared the manuscript. RR ran simulation and produced results. SB did analysis and contributed to the manuscript preparation. SAR contributed in the manuscript preparation.

Competing interests. The authors have no competing interests.

Acknowledgements. The IITM Pune is funded by the Ministry of Earth Science (MoES) , Government of India. The simulations were carried out on HPC facility 'Aaditya' (http://aadityahpc.tropmet.res.in/Aaditya/index.html) provided by MoES. This research is partially supported by the NSERC-Hydro-Quebec Industrial Research Chair program to M.K. Yau. The authors would like to thank Mr. Manmeet Singh, CCCR, IITM for a productive discussion on machine learning algorithms for this work.

References

Ayala, O., Rosa, B., Wang L.P. and Grabowski, W. W.: Effects of turbulence on the geometric collision rate of sedimenting droplets. Part 1. Results from direct numerical simulation, New J. Phy., 10(7), p. 075015. doi: 10.1088/1367-2630/10/7/075015, 2008.

Baker, M. B., and Latham, J.: The Evolution of Droplet Spectra and the Rate of Production of Embryonic Raindrops in Small Cumulus Clouds: . Journal of the Atmospheric Sciences, 36(8), 1612-1615, 1979.

Bengtsson, L.: The global atmospheric water cycle, IOP Publishing Ltd, 5, 025202. doi:doi.org/10.1088/1748-9326/5/2/025202, 2010.

Bera, S.: Droplet spectral dispersion by lateral mixing process in continental deep cumulus clouds, J. Atmos. and Solar-Terrestrial Phys., 214, 105550, ISSN 1364-6826, doi: 10.1016/j.jastp.2021.105550, 2021.

Bera, S., Prabha, T. V. and Grabowski, W. W.: Observations of monsoon convective cloud microphysics over India and role of entrainment-mixing, J. Geophys. Res.: Atmospheres, 121(16), 9767–9788. doi: 10.1002/2016JD025133, 2016.

Bock, H. H.: Clustering Methods: A History of K-Means Algorithms, in Brito, P. et al. (eds) Selected Contributions in Data Analysis and Classification. Berlin, Heidelberg: Springer Berlin Heidelberg, 161–172. doi: 10.1007/978-3-540-73560-1_15, 2007.

Brenguier, J., and Chaumat, L.: Droplet Spectra Broadening in Cumulus Clouds. Part I: Broadening in Adiabatic Cores, Journal of the Atmospheric Sciences, 58(6), 628-641, 2001.

Chen, S. Bartello, P., Yau, M.K, Vaillancourt, P.A., and Zwijsen,K.: Cloud Droplet Collisions in Turbulent Environment: Collision Statistics and Parameterization, J. Atmos. Sci., 73(2), 621–636. doi: 10.1175/JAS-D-15-0203.1, 2016.

Clift, R., Grace, J.R., and Weber, M.E.: Bubbles, Drops, and Particles:Dover Publications, Incorporated, 2013.

Cooper, W. A., Baumgardner, D. and Dye, J. E.: Evolution of the droplet spectra in Hawaiian orographic clouds. In: Preprints AMS Conf. Cloud Phys., Snowmass, 52-55, 1986.

Cooper, W. A.: Effects of Variable Droplet Growth Histories on Droplet Size Distributions. Part I: Theory, J. Atmos. Sci., 46(10), 1301–1311. doi: 10.1175/1520-0469(1989)046<1301:EOVDGH>2.0.CO;2, 1989.

Devenish, B.J., Bartello, P. Brenguier, J.L., Collins, L.R., Grabowski, W.W., IJzermans, R. H. A., Malinowski, S.P., Reeks, M.W., Vassilicos, J.C., Wang, L.P. and Warhaft, Z.: Droplet growth in warm turbulent clouds, Q. J. Roy. Meteor. Soc., 138(667), 1401–1429. doi: 10.1002/qj.1897, 2012.

Franklin, C. N., Vaillancourt, P.A., Yau, M.K., and Bartello, P.: Collision Rates of Cloud Droplets in Turbulent Flow, J. Atmos. Sci., 62(7), pp. 2451–2466. doi: 10.1175/JAS3493.1, 2005.

Grabowski, W. W. and Paul Vaillancourt,: Comments on Preferential concentration of cloud droplets by turbulence: Effects on the early evolution of cumulus cloud droplet spectra, J. Atmos Sci, pp. 1433–1436. doi: 10.1175/1520-0469(1999)056<1433:COPCOC>2.0.CO;2, 1999.

Grabowski, W. W. and Petch, J. C.: Clouds in the Perturbed Climate System: Their Relationship to Energy Balance, Atmospheric Dynamics, and Precipitation. Struengmann Forum Report, in DEEP CONVECTIVE CLOUDS. NCAR, USA: Opensky. Available at: https://opensky.ucar.edu/islandora/object/books:211, 2009.

Grabowski, W. W. and Wang, L.P.:Growth of Cloud Droplets in a Turbulent Environment, Ann. Rev. Fluid Mech., 45(1), 293–324. doi: 10.1146/annurev-fluid-011212-140750, 2013.

Harrison, E. F., Minnis P., Barkstrom, B.R., Ramanathan V., Cess, R.D., Gibson, G.G.: Seasonal variation of cloud radiative forcing derived from the Earth Radiation Budget Experiment, J. Geophys. Res.: Atmospheres, 95(D11), 18687–18703. doi: 10.1029/JD095iD11p18687, 1990.

Gerber, H.E., Frick, G.M., Jensen, James G. Hudson, J.G.:Entrainment, Mixing, and Microphysics in Trade-Wind Cumulus, Journal of the Meteorological Society of Japan. Ser. II, 86A, 87-106.

Holton, J. R. and Hakim, G. J.: An Introduction to Dynamic Meteorology (Fifth Edition), Academic Press, ISBN 9780123848666. https://doi.org/10.1016/B978-0-12-384866-6.00039-8, 2013.

Jimenez, J., A. A. Wray, P. G. Saffman, and R.. S. Rogallo, 1993: The structure of intense vorticity in isotropic turbulence. J. Fluid Mech., 255, 65–90.

Jonas, P.: Growth of droplets in cloud edge downdraughts, Q. J. Roy. Meteor. Soc., 117(497), pp. 243–255. doi: https://doi.org/10.1002/qj.49711749711, 1991.

Jonas P. R.: Turbulence and Cloud Microphysics, Elsevier, 40(2–4), 283–306. doi: https://doi.org/10.1016/0169-8095(95)00035-6, 1996.

Karpinska, K., Bodenschatz, J. F., Malinowski, S. P., Nowak, J. L., Risius, S., Schmeissner, T., Shaw, R., Siebert, H., Xi, H., Xu, H., and Bodenschatz, E.: Turbulence-induced cloud voids: observation and interpretation: Atmospheric Chemistry and Physics, 19(7), 4991-5003, 2019.

A. Khain, M. Pinsky, T. Elperin, N. Kleeorin, I. Rogachevskii, A. Kostinski: Critical comments to results of investigations of drop collisions in turbulent clouds', Atmospheric Research, 86, 1–20. doi: 10.1016/j.atmosres.2007.05.003, 2007.

Kumar, B., Götzfried, P., Suresh, N., Schumacher, J., Shaw R. A. (2018): Scale Dependence of Cloud Microphysical Response to Turbulent Entrainment and Mixing, J. of Adv. Model. Earth Sy., 10(11), 2777–2785. doi: 10.1029/2018MS001487, 2018.

Kumar, B., S. Bera, Prabha, T.V. and Grabowski, W. W., : Cloud-edge mixing: Direct numerical simulation and observations in Indian Monsoon clouds', J. Adv. Model. Earth Sys., 9(1), 332–353. doi: https://doi.org/10.1002/2016MS000731, 2017.

Kumar, B., Schumacher, J. and Shaw, R. A. : Lagrangian Mixing Dynamics at the Cloudy-Clear Air Interface, J. Atmos. Sci., 71(7), 2564–2580. doi: 10.1175/JAS-D-13-0294.1,2014.

Kumar, B., Janetzko, F., Schumacher, J., and Shaw, R. A.: Extreme responses of a coupled scalar–particle system during turbulent mixing, New Journal of Physics, 14(11), 115020. doi: 10.1088/1367-2630/14/11/115020, 2012.

Latham, J. and Reed, R. L. : Laboratory studies of the effects of mixing on the evolution of cloud droplet spectra, Quarterly Journal of the Royal Meteorological Society, 103(436), 297–306. doi: 10.1002/qj.49710343607, 1997.

Lehmann, K., Siebert, H. and Shaw, R. A.: Homogeneous and Inhomogeneous Mixing in Cumulus Clouds: Dependence on Local Turbulence Structure, J. Atmos. Sci., 66(12), 3641–3659. doi: 10.1175/2009JAS3012.1, 2009.

Lu, C., Liu, Y., Niu, S., Krueger, S., and Wagner, T. (2013), Exploring parameterization for turbulent entrainment-mixing processes in clouds, J. Geophys. Res. Atmos., 118, 185– 194, doi:10.1029/2012JD018464

Luo, S., Lu, C., Liu, Y., Bian, J., Gao, W., Li, J., et al.:Parameterizations of entrainment-mixing mechanisms and their effects on cloud droplet spectral width based on numerical simulations, ournal of Geophysical Research: Atmospheres, 125, https://doi.org/10.1029/2020JD032972, 2020.

Lian, H., Charalampous, G. and Hardalupas, Y.: Preferential concentration of poly-dispersed droplets in stationary isotropic turbulence, Exper. Fluids, 54. doi: 10.1007/s00348-013-1525-3, 2013.

Pedregosa, F.: Scikit-learn: Machine Learning in Python', Journal of Machine Learning Research, 12(85), 2825–2830, 2011.

Pinsky, M., Khain, A. and Shapiro, M.,: Stochastic effects of cloud droplet hydrodynamic interaction in a turbulent flow, Atmos. Res., 53, pp. 131–169. doi: 10.1016/S0169-8095(99)00048-4, 2000.

Pruppacher, H. R. and Klett, J.D.: Microphysics of Clouds and Precipitation, Springer. Available at: https://www.springer.com/gp/book/9780792342113, 1997.

Randall, D. A. and Tjemkes, S. : Clouds, the earth's radiation budget, and the hydrologic cycle, Global and Planetary Change, 4(1), 3–9. doi: 10.1016/0921-8181(91)90063-3, 1991.

Riemer, N. and Wexler, A. S.: Droplets to Drops by Turbulent Coagulation, J. Atmos. Sci., 62(6), 1962–1975. doi: 10.1175/JAS3431.1, 2005.

Rogers, R. R. and Yau, M. K. (1996), A Short Course in Cloud Physics. Elsevier, 1996.

Shaw R. A.: Particle-turbulence interactions in atmospheric clouds, Annu. Rev. Fluid Mech., 35(1), 183–227. doi: 10.1146/annurev.fluid.35.101101.161125, 2003.

Shaw, R. A., Reade, W. C., Collins, L. R., and Verlinde, J.: Preferential Concentration of Cloud Droplets by Turbulence: Effects on the Early Evolution of Cumulus Cloud Droplet Spectra., J. Atmos. Sci., 55, 1965–1976. doi: 10.1175/1520-0469(1998)055<1965:PCOCDB>2.0.CO;2, 1998.

SIONLib: Scalable I/O library for parallel access to task-local files. Germany: Forschungszentrum Jülich. Available at: https://www.fz-juelich.de/ias/jsc/EN/Expertise/Support/Software/S IONlib/_node.html.

Squires, K. D., and J. K. Eaton, 1991: Measurements of particle dispersion obtained from direct numerical simulations of isotropic turbulence. J. Fluid Mech.,226, 1–35.

Vaillancourt, P.A., Yau, M.K., Bartello, P., and Grabowski, W.W.: Microscopic Approach to Cloud Droplet Growth by Condensation. Part II: Turbulence, Clustering, and Condensational Growth, J. Atmos. Sci., 59(24), 3421–3435. doi: 10.1175/1520-0469(2002)059<3421:MATCDG>2.0.CO;2, 2002.

Vaillancourt, P. A. and Yau, M. K.: Review of Particle-Turbulence Interactions and Consequences for Cloud Physics', B. Am. Meteor. Soc., 81(2), 285–298. doi: 10.1175/1520-0477(2000)081<0285:ROPIAC>2.3.CO;2, 2000.

Vaillancourt, P. A., Yau, M. K. and Grabowski, W. W.: Upshear and Downshear Evolution of Cloud Structure and Spectral Properties, Am. Meteor. Soc., 54(9), 1203–1217. doi: 10.1175/1520-0469(1997)054<1203:UADEOC>2.0.CO;2, 1997.